UPPSALA
UNIVERSITET

FYSMAS1043

Examensarbete 30 hp
Augusti 2016

Magnetocrystalline Anisotropy in $(Fe_xNi_{1-x})_2B$ Materials

Anders Stangel
Supervisor: Jan Rusz

Masterprogrammet i fysik
Master Programme in Physics

Anders Stangel

Magnetocrystalline Anisotropy in $(Fe_xNi_{1-x})_2B$ Materials

UPPSALA
UNIVERSITET

Abstract

The magnetic properties of the $(Fe_xNi_{1-x})_2B$ family of materials are explored using DFT calculations utilizing the FPLO and SPR-KKR code packages. It is found that a uniaxial magnetocrystalline anisotropy exists at around $x = 0.8$ with a magnetocrystalline anisotropy energy at around $0.3\frac{MJ}{m^3}$. A calculation of the lattice constant for these materials were attempted but failed due to the emergence of local minima and the calculations of magnetic properties were instead done using lattice parameters interpolated between known experimental values.

Sammanfattning

Permanentmagneter och magnetiska material har varit kända sedan antiken, då i form av naturliga permanentmagneter som till exempel magnetit. Användningsområdena då innefattade bland annat kompassen eller helt enkel som en besynnerlig leksak. I modern tid har dock nya användningsområden för magetiska material dykt upp, till exempel inom elekriska motorer, vindkraftverk och hårddiskar. Dessa användningsområden har för med sig krav på kraftfullare magnetiska material än vad som behövts tidigare.

Flera exempel på kraftfulla permanent magneter existerar redan. De flesta av dessa använder sig av sällsynta jordartsmetaller som neodym och samarium. Sådana material har länga uppfyllt alla krav industrin har ställt på sina permanentmagneter men de senaste åren har priset på dessa ämnen gått upp kraftigt vilket har skapat ett behov av material som uppfyller industrins krav på prestanda utan att innehålla sällsynta jordartsmetaller.

Två av de egenskaper som är intressanta för en permanentmagnet är magnetisk mättnad, som är ett mått på hur kraftfull magneten är, och koercivitet som är ett mått på hur väl magneten står emot yttre magnetiska fält utan att dess magnetiska egenskaper försämras. Koerciviteten hos ett material kan i sin tur räknas ut med hjälp av materialets magnetokristallina anisotropienergi (MAE) som är den mängd energi som behövs för att vrida det magnetiska fältet från sin naturliga riktning till den riktning som är svårast att uppnå för materialet. Denna egenskap har också fördelen att den kan säga oss något om huruvida materialet är magnetisk i en specifik rikting alls eller om den naturliga riktningen för det magnetiska fältet är utspritt över flera möjliga riktningar vilket skulle göra materialet oanvändbart som permanentmagnet.

I den här rapporten använder vi matematiska metoder för att räkna ut magnetisk mättnad och MAE för en familj material bestående av bor förenat med en blandning av järn och nickel vilket ger den kemiska formeln $(\mathrm{Fe_xNi_{1-x}})_2\,\mathrm{B}$. Denna familj material har fördelen att alla beståndsdelar i materialet är billiga. Vi hittade ett område kring 80% järn där både den magnetiska mättnaden och MAE är tillräckligt höga för att ämnena ska vara intressanta att studera närmare.

Acknowledgements

I would like to thank my supervisor Jan Rusz for his patient guidance through the making of this work. In addition to him I want to thank Alexander Edström and Mirosław Werwiński for their assistance in learning how to use the code packages SPR-KKR and FPLO as well as giving invaluable input on the thesis itself and my friends and family for all their love and support.

Contents

1. Introduction & Motivation

The field of permanent magnet materials is one that has been extensively studied, both because of the complexities in the field and because of their applications in a wide number of fields ranging from electric motors, generators, turbines, data storage devices, maglev transport and breaks in amusement parks [1]. With these industries comes a demand for high-performance permanent magnets. Several such high-performing permanent magnets already exist and in particular magnets including rare-earth metals and transition metals have shown to have magnetic properties superior to all known alternatives. The fact that no other materials seemed to be able to compete with materials such as $SmCo_5$ and $Nd_2Fe_{14}B$ long made these materials the primary options for industrial applications, having all the desired properties that the industry needed out of a permanent magnet.

The price of the raw materials has proven to be another property that the industry needs to take into account however and these rare-earth metals have in recent years become less desirable for economic and political reasons [1, 2, 3, 4], and thus there is still a need for the development of new permanentmagnetic materials, in particular materials that do not include rare-earth metals. In searching for such a magnet the properties that need to be considered are the Curie temperature and the energy product, the latter of which requires a large saturation magnetization and magnetocrystalline anisotropy energy (MAE) to get coercivity. Several existing materials can already compete with the strong rare-earth magnets for Curie temperatures and saturation magnetization. These materials include the transition metals such as bcc Fe and hcp Co. However, in these the MAE is lower by one or more orders of magnitude compared to the rare-earth magnets. For bcc Fe this low MAE can be explained by the inherent symmetry in the bcc structure where the magnetic moments have many possible directions that are equivalent and the spin-orbit coupling being main source of magnetic anisotropy is generally lower in high symmetry crystals as long as perturbation theory holds. Other materials are thus needed that fulfil the need for strong and stable permanent magnets made from cheaper elements than the rare-earth metals. Materials with lower symmetry more easily lend themselves to magnetic anisotropy and higher spin orbit coupling. One example of such symmetry breaking occurs in materials with a tetragonal lattice structure rather than a cubic one like bcc Fe, since in such a material, where the lattice constants fulfil $c \neq a = b$ a magnetic moment along the z-axis and a magnetic moment along the plane orthogonal to the z-axis is not symmetrically equivalent. Such a material could be of interest

provided it shows easy axis magnetization rather than easy plane magnetization.

A group of potential candidates stem from the family of materials based on Fe_2B which is known to have an tetragonal structure [5]. Fe_2B has both a high total magnetic moment per unit volume and a high MAE but the magnetic anisotropy is not uniaxial and is thus useless for applications. However, by alloying this material with other elements it has been shown to have a uniaxial magnetic anisotropy. For example alloying Fe_2B with cobalt to become $(Fe_xCo_{1-x})_2B$ does for certain values of x have both a uniaxial magnetic anisotropy and a sufficient MAE to make it interesting for further studies [5, 6, 7, 8].

Another material that has been considered for alloying with Fe in Fe_2B is nickel. The alloy $(Fe_xNi_{1-x})_2B$ has been shown [5] to have a tetragonal structure for all values of x. Nickel serves as a complement to cobalt based alloys because of the relative cheaper cost of nickel compared to cobalt. This material does show low magnetic moment for high concentrations of nickel [5] but may have uniaxial magnetic anisotropy for lower concentrations of nickel and as such it is still a material of interest for study.

In this work the magnetization and MAE of $(Fe_xNi_{1-x})_2B$ will be studied for selected values of x using density functional theory (DFT), in order to determine if the material for some concentration of Ni exhibits uniaxial magnetic anisotropy and if so if the magnetization and MAE is large enough for industrial applications. The density of states and bandstructure of selected values of x is presented as a framework to discuss the nature of this family of materials. The theory of magnetism will be discussed in chapter 2 to the extent relevant for this study. In chapter 3 an overview of the specific computational methods used in the study will be presented and finally in chapters 4 and 5 the results of the study will be presented and discussed respectively, in addition to a brief discussion on potential future studies based on the findings.

2. Theory

Here the relevant theory and mathematical background is presented. The theory of magnetism with spin-orbit coupling and the arising of magnetic anisotropy is presented and finally the mathematical treatment and relevant approximations of DFT and the approximations used to treat random alloying are outlined.

2.1 Theory of magnetism, relativistic electrons and spin-orbit coupling

The spontaneous magnetic field of a material arises due to the spin and the orbital angular momentum of the material's electrons, each of the quantum numbers providing a contribution to the total magnetic moment. The Schrödinger equation of a wave function Ψ

$$\hat{H}\Psi(\mathbf{x}) = E\Psi(\mathbf{x}), \tag{2.1}$$

where $\hat{H}$ is the Hamiltonian operator gives a non-relativistic description of the electrons in a system. In the early days of quantum mechanics experiments showed that the electrons had twice the expected number of allowed states. To solve this, spin was introduced to account for these extra states [9, 10]. While trying to work out relativistic quantum mechanics Dirac [11, 12] introduced the relativistic equation

$$\begin{aligned}\left[i\frac{\partial}{\partial t} + eA_0 + \gamma_1\left(i\frac{\partial}{\partial x_1} + eA_1\right) + \gamma_2\left(i\frac{\partial}{\partial x_2} + eA_2\right)\right.\\ \left.+\gamma_3\left(i\frac{\partial}{\partial x_3} + eA_3\right) + \gamma_0 m\right]\psi = 0\end{aligned} \tag{2.2}$$

in natural units or written in another way

$$\left(\gamma^\mu\left(i\partial_\mu - eA_\mu\right) - m\right)\psi = 0. \tag{2.3}$$

A_μ here are arbitrary electromagnetic fields of potential, γ^μ are the Dirac matrices and e and m are the electron charge and mass respectively. From here the spin appeared as an internal angular momentum in addition to the orbital angular momentum in order to preserve Lorenz invariance. Equation 2.3 does

accurately describe spin-orbit coupling [13] giving rise to the effective magnetic magnetocrystalline anisotropy . Equation 2.3 can after separating out time independence be written as the Kohn-Sham-Dirac equations [14]

$$\left[-i\alpha\nabla+\beta m+A^{\text{eff}}-\varepsilon_i\right]\phi_i(\mathbf{r})=0 \tag{2.4}$$

where $\mathbf{A}^{\text{eff}}$ is the effective magnetic vector potential, $\phi_i(\mathbf{r})$ are the eigenfunctions of the Kohn-Sham equations described further in section 2.3 and α and β are the Dirac matrices. A^{eff} can then be given as a functional of exchange and correlation energies [14].

$$\begin{aligned} A^{\text{eff}} = &-\left(V^{\text{ext}}(\mathbf{r})+e^2\int\frac{n(\mathbf{r}')}{|\mathbf{r}-\mathbf{r}'|}d\mathbf{r}'+\frac{\delta E_{\text{xc}}^{\text{R}}}{\delta n(\mathbf{r})}\right)I \\ &-e\alpha\left(A^{\text{ext}}(\mathbf{r})+e\int\frac{J(\mathbf{r}')\,d\mathbf{r}'}{|\mathbf{r}-\mathbf{r}'|}+\frac{\delta E_{\text{xc}}^{\text{R}}}{\delta J(\mathbf{r})}\right) \end{aligned} \tag{2.5}$$

Note the similarities between equations 2.5 and the potential terms in equations 2.17 and 2.21. This functional appearance of the potentials will be further discussed in section 2.3.

This formalism treats the spin-orbit coupling and the scattering spin polarization on equal footing. Depending on the material it is possible to get the same accuracy with less computation power by treating one of them variationally or as a perturbation to a scalar relativistic approximation that otherwise would lack a spin-orbit coupling term [15] where the added a spin-orbit coupling term becomes [16]

$$H_{\text{SOC}}=\frac{c^2}{\left(2c^2-V\right)^2}\boldsymbol{\sigma}\cdot(\nabla V\times\mathbf{p}), \tag{2.6}$$

which can be taken along with other relativistic effects such as the mass-velocity enhancement [17]

$$H_{\text{mv}}=-\frac{p^4}{8m^3c^2} \tag{2.7}$$

and the Darwin term [18].

$$H_{\text{Darwin}}=\frac{e\nabla^2V}{8c^2m^2} \tag{2.8}$$

In this work fully relativistic calculations will be performed for of all electronic state and magnetization calculations.

2.2 Magnetic anisotropy

Magnetic anisotropy is the directional energy dependence of the magnetic moment in a material in the absence of an external magnetic field. This directional dependence is determined by a vast number of factors including morphology, chemical composition, alloying order of the material in addition to any surface, interface or impurities. In this work, a perfect crystal without impurities, surfaces and interfaces is assumed and these effects are thus not taken into consideration. While many different kinds of magnetic anisotropy exists [19] the two most discussed kinds are magnetocrystalline anisotropy and shape anisotropy. In this work the focus will be on magnetocrystalline anisotropy.

The magnetic anisotropy is often expressed in terms of the anisotropy constants K_i for $i = 1, 2, 3, \cdots$ so that magnetic anisotropy can be expressed as

$$E = E_{\text{iso}} + \sum_i c_i K_i, \tag{2.9}$$

where c_i depends on the direction of the magnetic moments and E_{iso} is the part of the energy that is not directionally dependent. For example in a uniaxial crystal the magnetic anisotropy can be expressed as

$$E = E_{\text{iso}} + K_1 \sin^2(\theta) + K_2 \sin^4(\theta) + K_3 \sin^6(\theta) \cos(6\phi) + \cdots, \tag{2.10}$$

where θ is the angle between the magnetization and the z-axis and ϕ is the azimuthal angle to the z-axis[3] and for a cubic crystal the magnetic anisotropy can be expressed as

$$E = E_{\text{iso}} + K_1 \left(\alpha_1^2\alpha_2^2 + \alpha_2^2\alpha_3^2 + \alpha_3^2\alpha_1^2\right) + K_2 \alpha_1^2\alpha_2^2\alpha_3^2 + K_3 \left(\alpha_1^2\alpha_2^2 + \alpha_2^2\alpha_3^2 + \alpha_3^2\alpha_1^2\right)^2 \cdots \tag{2.11}$$

where α_i is the cosine of the angle with respect to the cubic axes. Both the anisotropy constants and the general structure of the magnetic anisotropy is thus obviously material dependent [20].

In this work materials with a uniaxial crystal structure will be studied so equation 2.10 would describe the magnetic anisotropy of this material if the values of K_i where known for all values of $i = 1, 2, 3, \cdots$. For the purposes of this work the magnetic anisotropy arises as a result of spin-orbit coupling outlined in section 2.1. The spin-orbit coupling however is a relativistic effect and needs to be more carefully treated [21, 22].

The MAE is then tied to the magnetic anisotropy stemming from the energy calculated for example in equation 2.10 or 2.11. The MAE is defined as the maximal difference in energy over the magnetization directions.

$$E_{\text{MAE}} = E(\theta, \phi)_{\max} - E(\theta, \phi)_{\min} \tag{2.12}$$

Note that the isotropic part E_{iso} always disappear in such an equation due to it being the same in both terms. As such the MAE is a measurement of the

stability of the magnetization direction in a material with a high MAE being needed for a good permanent magnet.

2.3 Density functional theory

All of the preceding is based on the interactions between a large number of electrons. This is dealt with in part by realizing that the system is a periodic infinite crystal and as such it can efficiently be treated through a Fourier transform. In the explicit method of summing up the interaction between every pair of electrons and ions the Hamiltonian would represent the total energy of the system from all those contributions of a system with M ions and N electrons

$$\hat{H} = -\frac{1}{2}\sum_{i=1}^{N}\nabla_i^2 - \frac{1}{2}\sum_{A=1}^{M}\frac{1}{M_A}\nabla_A^2 - \sum_{i=1}^{N}\sum_{A=1}^{M}\frac{Z_A}{r_{iA}} + \sum_{i=1}^{N}\sum_{j>i}^{N}\frac{1}{r_{ij}} + \sum_{A=1}^{M}\sum_{B>A}^{M}\frac{Z_A Z_B}{R_{AB}} \tag{2.13}$$

where M_A and Z_A is the mass and atomic number of ion A and $e = 1$[23]. Dealing with these interactions between each electron pair separately and coupling the electrons and ions will prove to be too computationally heavy for any large system. One method that has been proven to be a powerful tool in calculating the ground state of materials is density functional theory (DFT).

DFT is an *ab initio* theory of matter and as such derives all its results from first principles without additional assumptions, having its roots in established quantum mechanics [23]. It starts from the non-relativistic Schrödinger equation representing the wave function Ψ in equation 2.1. The kinetic term from the ions in equation 2.13 disappears under the Born-Oppenheimer approximation but since the calculations still scale with the number of atoms in the system it is still clear that this yields unfeasibly large calculations for large systems. In addition to that, the electrons in a magnetic system cannot be treated as non-relativistic as explained in section 2.1. A reasonable attempt would be to try and generalize the many-body problem for the non relativistic case in such a way that it can be extended into the relativistic case.

The Hamiltonian in equation 2.13 can be rewritten with the different types of interaction specified.

$$\hat{H} = \left(-\frac{\hbar^2}{2m}\sum_{i=1}^{N}\nabla_i^2 + \sum_{i}^{N} V_{\text{ext}}(\mathbf{r}_i) + \frac{1}{2}\sum_{i\neq j}^{N} w(|\mathbf{r}_i - \mathbf{r}_j|) \right) \tag{2.14}$$

where $V_{\text{ext}}(\mathbf{r})$ is the external potential, which in equation 2.13 corresponds to the interactions with the ions, and $w(|\mathbf{r}_i - \mathbf{r}_j|)$ is the Coulomb interaction between two electrons at sites i and j. While equation 2.14 removes the need to sum up the ions for any other purpose than to determine $V_{\text{ext}}(\mathbf{r})$ it still requires explicit summation over the electrons. This problem has been treated in

different ways, including the Hartree-Fock theory that treated the many body problem as a set of equations with a Slater determinant of one particle wave functions [24]. The Hartree-Fock theory could not account for correlation effects in the system however [25] and other methods became necessary. DFT got its foundation in the first Hohenberg-Kohn theorem which showed that the total energy ground state could be uniquely determined from the electron density [26, 23] And that the energy could be written as a functional of the electron density in a static potential v

$$E[n] = \int V_{\text{ext}}(\mathbf{r}) n(\mathbf{r}) d\mathbf{r} + \frac{1}{2} \int \int \frac{n(\mathbf{r}) n(\mathbf{r}')}{|\mathbf{r} - \mathbf{r}'|} d\mathbf{r} d\mathbf{r}' + G[n], \tag{2.15}$$

where n is the electron density and $G[n]$ is a universal functional of the electron density [26]. The correlation effects missing from the Hartree-Fock theory show up in equation 2.15 in the univeral functional $G[n]$

$$G[n] \equiv T_{\text{s}}[n] + E_{\text{xc}}[n]. \tag{2.16}$$

T_{s} here is the kinetic energy functional and $E_{\text{xc}}[n]$ is the exchange-correlation functional which can in turn be divided into an exchange and a correlation part [25]. The Hohenberg-Kohn theorem allows the system to be reduced from a many-body problem to a single particle problem using the Kohn-Sham approach where the system is set up as a system of equations.

$$\left[-\frac{1}{2}\nabla^2 + V_{\text{ext}}(\mathbf{r}) + \int \frac{n(\mathbf{r}')}{|\mathbf{r} - \mathbf{r}'|} d\mathbf{r}' + \frac{\delta(n\varepsilon_{\text{xc}}(n))}{\delta n} \right] \psi_i(\mathbf{r}) = \varepsilon_i \psi_i(\mathbf{r}), \tag{2.17}$$

for a local potential [25]. Here ε_{xc} is the exchange-correlation energy per particle in the system. Equation 2.17 has a kinetic term and several potential terms including the external potential that can be expressed as an effective potential of the system.

$$V_{\text{eff}} = V_{\text{ext}}(\mathbf{r}) + \int \frac{n(\mathbf{r}')}{|\mathbf{r} - \mathbf{r}'|} d\mathbf{r}' + \frac{\delta(n\varepsilon_{\text{xc}}(n))}{\delta n} \tag{2.18}$$

Of these terms V_{ext} is assumed to be known from the system and $\int \frac{n(\mathbf{r}')}{|\mathbf{r}-\mathbf{r}'|} d\mathbf{r}'$ is a known quantity as long as $n(\mathbf{r})$ is known. $n(\mathbf{r})$ can be calculated using a starting guess and then using an iterative process until self-consistency is achieved. Methods for this are discussed in section 3.1 and 3.2. The only unknown term thus stems from the exchange correlation potential.

$$V_{\text{xc}} = \frac{\delta(n\varepsilon_{\text{xc}}(n))}{\delta n}, \tag{2.19}$$

which is a quantity that needs to be treated separately. Note that the ground state electron density in this system can be expressed by the Kohn-Sham orbitals themselves.

$$n(\mathbf{r}) = \sum_{i=1}^{N} |\psi_i(\mathbf{r})|^2 \tag{2.20}$$

where the sum is over the N lowest energy states. The many-body problem of several electrons has thus been reduced to a single body problem with several eigenstates.

This approach so far has assumed a local external potential. It is possible to extend the Hohenberg-Kohn theorem to non-local potentials as well [27] without the loss of universality in the energy functionals and this non-locality has to be treated separately. Here the potential V_{xc} and thus the functional that describes it can be divided into an exchange part and a correlation part so that

$$\left(-\frac{1}{2}\nabla^2 + V_{\text{ext}}(\mathbf{r}) + \int \frac{n(\mathbf{r}')}{|\mathbf{r}-\mathbf{r}'|}d\mathbf{r}' + \frac{\delta(n\varepsilon_{\text{c}}(n))}{\delta n}\right)\psi_i - \int \frac{n_1(\mathbf{r},\mathbf{r}')}{|\mathbf{r}-\mathbf{r}'|}\psi_i(\mathbf{r}')d\mathbf{r}' = \varepsilon_i\psi_i(\mathbf{r}), \tag{2.21}$$

where ε_c is the correlation energy per particle in the system and n_1 is the overlap between wave-functions at different sites [25].

$$n_1(\mathbf{r},\mathbf{r}') = \sum_{i=1}^{N} \psi(\mathbf{r})\,\psi^*(\mathbf{r}') \tag{2.22}$$

As can be seen from equations 2.21 and 2.22 this approach does not add any new unknown quantities to the system, though it changes V_{xc} to V_c. Provided that these quantities can be known exactly this approach would yield an exact result.

In practice however this is not the case apart from a few rare exceptions and approximations need to be done. The most basic of these approximations is the local density approximation (LDA) where the exchange-correlation functional E_{xc} is expressed purely in terms of the density itself, treating E_{xc} like in a homogenous electron gas in every point [28]. This approximation can also be expanded to differ between the density of electrons with spin up and electron with spin down where $n(\mathbf{r}) = n(\mathbf{r})_{\uparrow} + n(\mathbf{r})_{\downarrow}$ leading to the local spin-density approximation (LSDA). Collectively these two approximations are known as the local (spin-) density approximation (L(S)DA) when discussing properties that the two approximations have in common. L(S)DA has shown to give acceptable results for calculations of molecular geometries and frequencies but lacks in calculations of binding energies since it tends to lead to overbinding in addition to miscalculating the exchange energy [28, 29] as well as underestimating the band gap in semiconductors and insulators [30]. One correction is to add the terms from the Coulomb interactions and exchange interactions

which are absent in the L(S)DA. This approximation is called LDA+U and provides an improvement over L(S)DA for strongly correlated systems such as can be found with rare-earth metal ions with partially filled f-shells or transition metals with partially filled d-shells [31]. Another approximation that has shown to be superior to L(S)DA for strongly correlated systems is the dynamic mean-field theory (DMFT) that changes the static mean field potential of previously mentioned DFT approximations for a dynamic potential [32]. Typically DMFT is used in a hybrid functional combining DMFT with LDA or another approximation [32, 33].

The generalized gradient approximation (GGA) takes LDA one step further by incorporating the gradients of the electron density in addition to the electron density itself. It is known to provide an overall improvement over LDA for many systems and properties though it can be found to slightly overestimate lattice constants [34]. In order to calculate magnetic properties of materials GGA too needs to go to spin-polarized DFT as was done going from LDA to LSDA with appropriate changes to the effective potential in equation 2.18. This has been shown to give calculations of satisfactory accuracy for calculations of magnetic properties of transition metals [35].

In this work the GGA model by Perdew, Burke and Ernzerhof (PBE) will be used since that has been shown to have a good accuracy for treatment of magnetic properties of 3d transition metals and compounds of 3d transition metals[36].

2.4 Treatment of randomly disordered alloys

Having a fundamental framework for dealing with many body systems such as solid matter including the particular material of interest here the only thing left is to deal with the alloying of the material. For a $(Fe_xNi_{1-x})_2B$ crystal where $x \neq 0$ and $x \neq 1$ the random instances of iron or nickel need to be treated. One way of treating the system is, by instead of doing calculations on small repeating unit cells, use the supercell approximation in which a supercell consisting of several unit cells with one or more disordered configuration with imposed periodic boundary conditions is taken as the periodic unit cell. In order to acquire accurate results with such a system many configurations would generally have to be considered [37] and while the supercell approximation would accurately describe the system for a large enough super cell it would thus prove to be computationally too heavy since it demands that a much larger space be considered explicitly. Some other approximation is thus needed to get viable computation methods. Here two such approximations will be considered.

2.4.1 VCA

The first approximation is the virtual crystal approximation (VCA). In VCA the alloyed sites are considered to be virtual atoms of the same species with an atomic number that is the average of the two alloyed species weighted depending on the value of x. So for an alloy with the proportions $X = A_{\mathrm{x}}B_{1-\mathrm{x}}$ in the VCA the alloy sites gets a single potential that is taken to be the average of the potentials from the alloyed elements, creating a virtual element at that site with potential [37]

$$V_{\mathrm{Virtual}} = \mathrm{x}V_{\mathrm{A}} + (1-\mathrm{x})\,V_{\mathrm{B}}, \tag{2.23}$$

and the virtual element is thus taken to have atomic number $Z_{\mathrm{Virtual}} = \mathrm{x}Z_{\mathrm{A}} + (1-\mathrm{x})\,Z_{\mathrm{B}}$. The non alloyed elements of the crystal can then take its normal potential giving a crystal such as $(\mathrm{Fe_xNi_{1-x}})_2\mathrm{B}$ in the calculation becomes $\mathrm{X_2B}$ where X is the virtual element put in place by the VCA.

The premise for this approximation is simple and its implementation is simple [38] and efficient [37]. Still the model is known to produce results of good accuracy for yielding wave functions and energy spectra in alloys [39] and spin and orbital moments [38, 40]. The nature of VCA does imply that the approximation is better for alloying elements which are neighbouring each other on the periodic table, such as alloying Fe and Co or Co and Ni [38], while giving a less accurate result for elements that are further apart in the periodic table, such as Fe and Ni. For the calculations needed for this study, VCA has shown to vastly overestimate the MAE of systems, though the MAE as a function of alloy concentration in an alloy can be expected to have qualitatively the right shape [40].

This work does utilize VCA to treat a disordered alloy of Fe and Ni and calculating the MAE using it with the FPLO method described in section 3.2 in spite of these well documented shortcomings. The MAE from these calculations are expected to be vastly overestimated, though the shape of the MAE as a function of alloy concentration is expected to be correct. It can thus be used to check for errors while using other methods like the SPR-KKR method described in section 3.1 which instead of VCA utilizes the coherent potential approximation (CPA) described in subsection 2.4.2. In addition to that, since the total energy as a function of the lattice parameters a and c is expected to be conceptually correct [41], FPLO can be utilized to perform lattice relaxation calculations where the exact total energy is less important than the values of the lattice parameters where the energy function has a minimum.

2.4.2 CPA

The second approximation that will be considered is the coherent potential approximation (CPA). In CPA the disorder is treated by adding impurities of the alloyed materials in an effective CPA medium [42] with the condition that

on average no scattering occurs for a single electron travelling in the CPA medium when a single CPA scattering matrix gets replaced with an atom specific scattering matrix of one of the alloyed types [43].

CPA is based on a Green's function approach [42]. A Green's function $G(\mathbf{x},\mathbf{x}')$ to an operator $f(\mathbf{x})$ fulfills

$$f(\mathbf{x})\,G\left(\mathbf{x},\mathbf{x}'\right)=\delta\left(\mathbf{x}-\mathbf{x}'\right), \tag{2.24}$$

where $\delta(\mathbf{x}-\mathbf{x}')$ is the Dirac delta. Here the Green's function in question is the Green's function to the Hamiltonian.

$$\left(E-\hat{H}\right)G\left(\mathbf{r},\mathbf{r}';E\right)=\delta\left(\mathbf{r}-\mathbf{r}'\right) \tag{2.25}$$

The Green's function of such a system is a powerful tool in electronic structure theory by defining the electron density [44, 45].

$$n(\mathbf{r})=-\frac{1}{\pi}\int_{-\infty}^{\mathrm{E_F}}\mathscr{I}G(\mathbf{r},\mathbf{r};E)\,dE \tag{2.26}$$

Naturally the Green's function depends on the elements involved in the alloy and their concentrations since it's defined by the Hamiltonian. The Green's function is the response function of the system [46] and is thus used in the t-matrix scattering approximation [47] defined by an implicit equation for an atom type α [42].

$$t^{\alpha}(E)=v^{\alpha}+v^{\alpha}G_0(E)\,t^{\alpha}(E), \tag{2.27}$$

where v^{α} is the perturbation potential for the atom type α and G_0 is the free electron Green's function. This total scattering matrix can be expressed in terms of the scattering path operators which includes all possible scattering events between cells n and m [47].

$$t(E)=\sum_{nm}\tau_{nm}(E) \tag{2.28}$$

A binary disordered alloy such as the alloy of Fe and Ni considered in this work has only site-diagonal elements considered in the disorder [48], and thus the only elements of the single site scattering operators are the case when $m=n$ which in terms of the scattering path operator can be expressed as a sum of the off-diagonal elements [45]

$$t_{nn}(E)=\sum_{i\neq n}\sum_{j\neq n}\tau_{ij}(E). \tag{2.29}$$

An effective CPA medium can then be taken to be a potential v_0 that has yet to be defined. All potentials belonging to the actual atoms can then be taken to be some perturbation to this CPA medium $v^{\alpha}=v_i-v_0$ where i is the atom

type and the unperturbed Green's function of the pure CPA medium system $\bar{G}$ can thus be defined through a Dyson equation [42].

$$\bar{G}_0 = G_0 + G_0 \left(\int v_0(\mathbf{x})\, dx \right) \bar{G}_0 \tag{2.30}$$

with G_0 defined as before. The CPA medium scattering operator $\bar{t}$ can then be defined with the perturbations v^α

$$\bar{t}^\alpha(E) = (v_i - v_0) + (v_i - v_0)\, \bar{G}_0(E)\, \bar{t}^\alpha(E), \tag{2.31}$$

and a CPA t matrix is obtained from the unperturbed system.

$$t^{CPA}(E) = v_0 + v_0 G_0(E)\, t^{CPA}(E) \tag{2.32}$$

So far, as long as v_0 and v_i are chosen correctly this is all exact. The approximation is then to assume that the paths are sufficiently long so that the concept of an average medium should provide a close enough approximation to the average path taken in the actual crystal [42]. The CPA scattering medium is then the weighted average of the scattering media of the pure crystals of respective alloying species [49].

$$\tau_{nn}^{CPA} = \sum_\alpha c_\alpha \tau_{nn}^\alpha, \tag{2.33}$$

where c_α is the concentration of element α and

$$(\tau_{nn}^\alpha)^{-1} = (t_{nn}^\alpha)^{-1} - \left(t_{nn}^{CPA}\right)^{-1} - \left(\tau^{CPA}\right)^{-1}. \tag{2.34}$$

From equations 2.33 and 2.34 CPA averaged Green's function can thus be obtained.

$$G^{\mathrm{CPA}}\left(\mathbf{r}, \mathbf{r}', E\right) = \sum_\alpha c_\alpha G^\alpha\left(\mathbf{r}, \mathbf{r}', E\right) \tag{2.35}$$

CPA is a more sophisticated approach than VCA and it gives a more accurate estimate of the MAE. While this CPA method fails in accounting for environmental effects or other such non-local effects except as an average [50] it can be expected to be accurate enough for all the electronic structure calculations considered in this work [39, 40, 51]. This work utilizes CPA within the SPR-KKR code package described in section 3.1.

3. Computational Methods

Here the computational methods will be discussed. First the code packages SPR-KKR and FPLO will be presented together with a brief outline of the underlying method. Then a theoretical background in methods to specifically calculate the MAE, DOS and band structure will be given.

3.1 SPR-KKR

The Spin Polarized Relativistic Korringa-Kohn-Rostocker method (SPR-KKR) is based on the works by Korringa [52], Kohn and Rostoker [53], also known as multiple scattering theory. The method utilizes the Green's functions of equation 2.25. The method utilizes the t matrix and scattering path operators outlined in 2.4.2 finding the scattering path operator as [54]

$$\tau^{nm}(E) = \left(t(E)^{-1} - g(E)\right)^{-1}_{nm} \tag{3.1}$$

for an electron at cite n with a scattering path to cite m and where $g(E)$ includes the structure constants of the system [47]. These can be retrieved through the unperturbed Green's function

$$G_0(\mathbf{r},\mathbf{r};E) = -ip\sum_L j_l(pr_<)\, h_l^+(pr_>)\, Y_L(\mathbf{r})\, Y_L^*\left(\mathbf{r}'\right) \tag{3.2}$$

where $p = \sqrt{E}$, $j_l(z)$ and $h_l^+(z)$ are the spherical Bessel and Hankel functions respectively and Y_L are spherical harmonics by using the scattering operator $T(E)$ and that can be retrieved from

$$T(E) = V(\mathbf{r}) + V(\mathbf{r})\, G_0(E)\, T(E) \tag{3.3}$$

where $V(\mathbf{r})$ is the potential of the system and the scattering operator is connected to the scattering path operator through [47]

$$T(E) = \sum_{nm} \tau^{nm}(E) \tag{3.4}$$

From equation 3.1 the scattering path operator can be used to calculate the Green's function through [49]

$$
\begin{aligned}
G\left(\mathbf{r},\mathbf{r}';E\right) = &\sum_{\Lambda\Lambda'} Z^n_\Lambda\left(\mathbf{r},E\right)\tau^{nn'}_{\Lambda\Lambda'}\left(E\right)Z^{n'\times}_{\Lambda'}\left(\mathbf{r}',E\right) \\
&-\sum_{\Lambda}\left(Z^n_\Lambda\left(\mathbf{r},E\right)J^{n\times}_\Lambda\left(\mathbf{r}',E\right)\Theta\left(\mathbf{r}'-\mathbf{r}\right)\right. \\
&\left.+J^n_\Lambda\left(\mathbf{r},E\right)Z^{n\times}_\Lambda\left(\mathbf{r}',E\right)\Theta\left(\mathbf{r}-\mathbf{r}'\right)\right)\delta_{nn'}.
\end{aligned}
\tag{3.5}
$$

where $Z^n_\Lambda\left(\mathbf{r},E\right)$ and $J^n_\Lambda\left(\mathbf{r}',E\right)$ are the regular and irregular solutions to the radial Schrödinger equaion. Using the Green's function the charge density is obtained from equation 2.26 and it is possible to calculate the dispersion relation $E\left(\mathbf{k}\right)$ as well as the spin magnetic moment

$$
\mu_{\text{spin}} = -\frac{\mu_\text{B}}{\pi}\Im\text{Tr}\int^{E_\text{F}} dE\int_V d^3r\beta\sigma_z G\left(\mathbf{r},\mathbf{r}';E\right) \tag{3.6}
$$

and orbital magnetic moment

$$
\mu_{orb} = -\frac{\mu_\text{B}}{\pi}\Im\text{Tr}\int^{E_\text{F}} dE\int_V d^3r\beta l_z G\left(\mathbf{r},\mathbf{r}';E\right) \tag{3.7}
$$

where $\beta=\gamma^0$ is the Dirac matrix of index zero, σ_z is the third Pauli matrix and l_z is the orbital angular momentum matrix.

This method lends itself well to the CPA approach described in section 2.4.2 by transforming the scattering path operator in equation 3.1 using the CPA equations given in equations 2.33 and 2.34 and then using the CPA medium to calculate a new Green's function from equation 2.35. The above formalism can then be utilized with the new Green's function as normal.

3.2 FPLO

The full potential local orbital (FPLO) method uses a real space representation of non-orthogonal local orbitals. The potential $v\left(\mathbf{r}\right)$ can be represented as

$$
v\left(\mathbf{r}\right) = \sum_{\mathbf{R}+\mathbf{s},L} v_{\mathbf{s},L}|\mathbf{r}-\mathbf{R}-\mathbf{s}|Y_L\left(\mathbf{r}-\mathbf{R}-\mathbf{s}\right), \tag{3.8}
$$

where $\mathbf{R}$ is the Bravais lattice vector, $\mathbf{s}$ is a basis vector for the unit cell and Y_L are the real spherical harmonics of orbital L to solve the Kohn-Sham equations and describe the density and potential while solving the Hartree potential using the Poisson equation [41] leaving only the exchange and correlation potential to be solved separately by decomposing them into parts centred at the lattice sites and vanishing quickly when approaching neighbouring sites [55]. This is accomplished by partitioning utilizing a shape function defined such that

$$
\sum_{\mathbf{R}+\mathbf{s}} f_s\left(\mathbf{r}-\mathbf{R}-\mathbf{s}\right) \equiv 1 \tag{3.9}
$$

and normalized according to

$$f_s(\mathbf{r}) = \frac{\prod_{\tau} H(-r)\left(\frac{\tau \mathbf{r}}{|\tau|^2}\right)}{\sum_{\tau}\prod_{\tau} H(\tau - r)\left(\frac{\tau(\mathbf{r}-\tau)}{|\tau|^2}\right)} \tag{3.10}$$

where $H(x)$ is the Heaviside step function and $\tau = \mathbf{R} - \mathbf{s}' - \mathbf{s}$ is a vector pointing to any point from the centre of a cell.

The Kohn-Sham equations are solved using the ansatz of the superposition of Bloch-states

$$|\mathbf{k}n\rangle = |\mathbf{R}\mathbf{s}L\rangle\, c_{L\mathbf{s}}^{\mathbf{k}n} e^{i\mathbf{k}(\mathbf{R}+\mathbf{s})} \tag{3.11}$$

The high localization of orbitals allows for splitting of valence and core orbitals where the core orbitals are so localized that the spherical average can be used in place of equation 3.8,

$$\left\langle \mathbf{R}'\mathbf{s}'L_c' | \mathbf{R}\mathbf{s}L_c \right\rangle = \delta_{L_c'Lc}\delta_{\mathbf{R}'+\mathbf{s}',\mathbf{R}+\mathbf{s}}, \tag{3.12}$$

where L_c are the core orbitals. The on-site electron density can then be calculated as a sum of the overlap densities from core orbitals, valence orbitals and the combination thereof [41].

$$n = \sum_{\mathbf{k}n}^{\mathrm{occ}} = |\mathbf{k}n\rangle\langle\mathbf{k}n| \tag{3.13}$$

$$n_{\mathbf{Rs}}^{\mathrm{on-site}} = n_{\mathbf{Rs}}^{\mathrm{on-site},cc} + n_{\mathbf{Rs}}^{\mathrm{on-site},cv} + n_{\mathbf{Rs}}^{\mathrm{on-site},vv} \tag{3.14}$$

where vv refers to overlap between valence orbitals and so on. In this work the FPLO method will be used in combination with VCA described in section 2.4.1 to treat disorder.

3.3 Calculating the Magnetocrystalline anisotropy energy and magnetic moment

In section 2.2, the magnetic anisotropy was discussed. Here the practical computations of the magnetic moment and the MAE will be presented.

The calculations of the magnetic moment is generally fairly straight forward since it falls out from spin polarized calculation of the electron density as

$$n(\mathbf{r}) = n_{\uparrow}(\mathbf{r}) + n_{\downarrow}(\mathbf{r}). \tag{3.15}$$

In the SPR-KKR method described in section 3.1 this relation falls out into equations 3.6 and 3.7. In the case of the FPLO method described in section

3.2 the magnetic moment is calculated directly from the SCF calculation of the electron density.

The MAE can be calculated as the maximum between two magnetization directions.

$$|E_{\mathrm{MAE}}| = |E(\hat{\mathbf{n}}_1) - E(\hat{\mathbf{n}}_2)| = |E_{\mathrm{min}} - E_{\mathrm{max}}|, \tag{3.16}$$

where $\hat{\mathbf{n}}_1$ is the preferred direction for the magnetization so that $E(\hat{\mathbf{n}}_1) = E_{\mathrm{max}}$and $\hat{\mathbf{n}}_2$ is the magnetization direction with the lowest energy. $E(\hat{\mathbf{n}}_2) = E_{\mathrm{min}}$. $\hat{\mathbf{n}}_1$ is called the easy axis and $\hat{\mathbf{n}}_2$ is called the hard axis. The sign for the MAE is decided according to some convention. One problem with this method for a general crystal is how to find the easy and the hard axes and thus the maximum and the minimum values for the MAE. This tends not to be a problem in practice since the preferred axis often is along a high symmetry axis in the crystal. In a uniaxial crystal for example the crystal generally has uniaxial magnetization with the easy axis being along the z-axis and the hard axis along the plane orthogonal to the z-axis or vice versa.

As long as $\hat{\mathbf{n}}_1$ and $\hat{\mathbf{n}}_2$ are the correct choices for the easy and the hard axes the total energy difference method will yield correct results by definition of E_{MAE}. Some care needs to be taken with the method since E_{MAE} tends to be very small compared to the value of E_{min} and E_{max}.

3.4 DOS and bandstructure

Quantum mechanics gives us the result that an electron in a material system cannot have any arbitrary energy. Instead it is confined to allowed energy levels. In a solid crystal these allowed states depend on the crystal momentum giving rise to a bandstructure.

The bandstructure of a material is the allowed energy levels as a function of crystal momentum. This is most notably expressed by finding the energy dispersion relation $E(\mathbf{k})$. In this work however the main focus will be on disordered alloys and the energy dispersion relation is replaced by the Bloch spectral function $A(\mathbf{k}, E)$ which reduces to the energy dispersion relation in the ordered limit. The Bloch spectral function can be expressed like a Fourier transform of the Green's function [21]

$$A(\mathbf{k}, E) = -\frac{1}{\pi N} \Im \mathrm{Tr} \sum_{n,n'}^{N} e^{i\mathbf{k}\left(\mathbf{R}_n - \mathbf{R}_{n'}\right)} \times \int_{\Omega} G(\mathbf{r} + \mathbf{R}_n, \mathbf{r} + \mathbf{R}_{n'}, E)\, d^3 r \tag{3.17}$$

The density of states (DOS) of a material is a measure of how many electron states is allowed per energy step in a crystal as a function of energy. The density of states is tied to the electron density $n(\varepsilon)$ through [56]

$$n = \int_V g(\varepsilon) f(\varepsilon) d\varepsilon \tag{3.18}$$

where $g(\varepsilon)$ is the density of states at energy ε, V is the volume of a primitive cell and $f(\varepsilon)$ is the Fermi function.

Equations 3.18 requires finite temperatures however and a way to define this function in the ground state is needed. In a Green's function method like SPR-KKR described in section 3.1 the density of states can be calculated using its ties to the Green's function described in section 2.4.2. Since the electron density can be calculated directly from the imaginary part of the Green's function using equations 2.26 and 3.18 the imaginary part of the Green's function $G(\mathbf{r}, \mathbf{r}, E)$ can be seen as a local density of states at site $\mathbf{r}$ [57]. From the equations 3.18 and 2.26 it can be seen that the imaginary part of the Green's function is tied to the density of states through the identity [58]

$$g(E) = -\frac{1}{\pi} \Im \mathrm{Tr} G_0(E) \tag{3.19}$$

for a system of non-interacting electrons and to add interaction add the interacting Green's function.

$$\delta g(E) = -\frac{1}{\pi} \Im \mathrm{Tr} \left(G_0(E) - G(E) \right) \tag{3.20}$$

This Lloyd's formula can be used to find the density of state [21, 58, 59]. Utilizing these methods to calculate the scattering matrices and Green's function, the density of states is obtained.

4. Results

Here the results of the study are presented. First the lattice constants, total magnetic moments and the MAE of the materials as a function of alloying concentration is plotted. Finally some DOS and band-plots of selected values of the alloying concentration are presented.

4.1 Lattice structure

Experimental lattice parameters at room temperature for Ni_2B, Fe_2B and $(Fe_{0.5}Ni_{0.5})_2B$ has previously been presented by Iga [5]. From these a lattice relaxation has been made using energy minimization with the FPLO package and the VCA described in sections 3.2 and 2.4.1 respectively. The accuracy is set to be within 1%

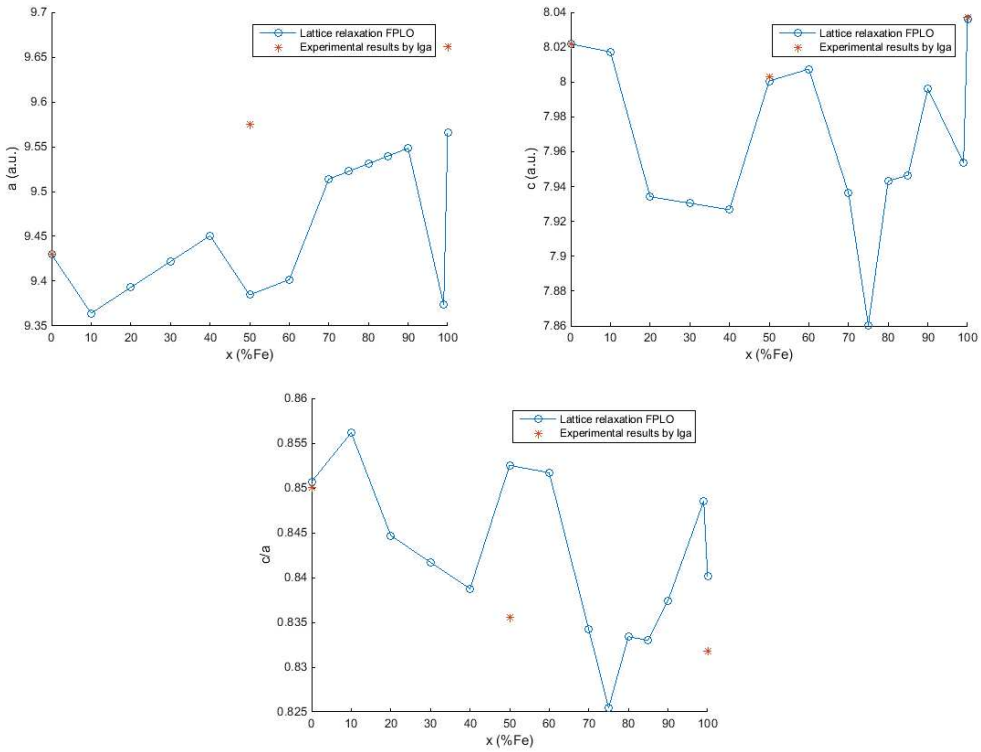

Figure 4.1. The lattice constants as a function of iron concentration and comparing with the experimental results by Iga [5].

Looking at figure 4.1 it is easy to see that the lattice relaxation calculations have not been successful. The expected result had been a smoother curve

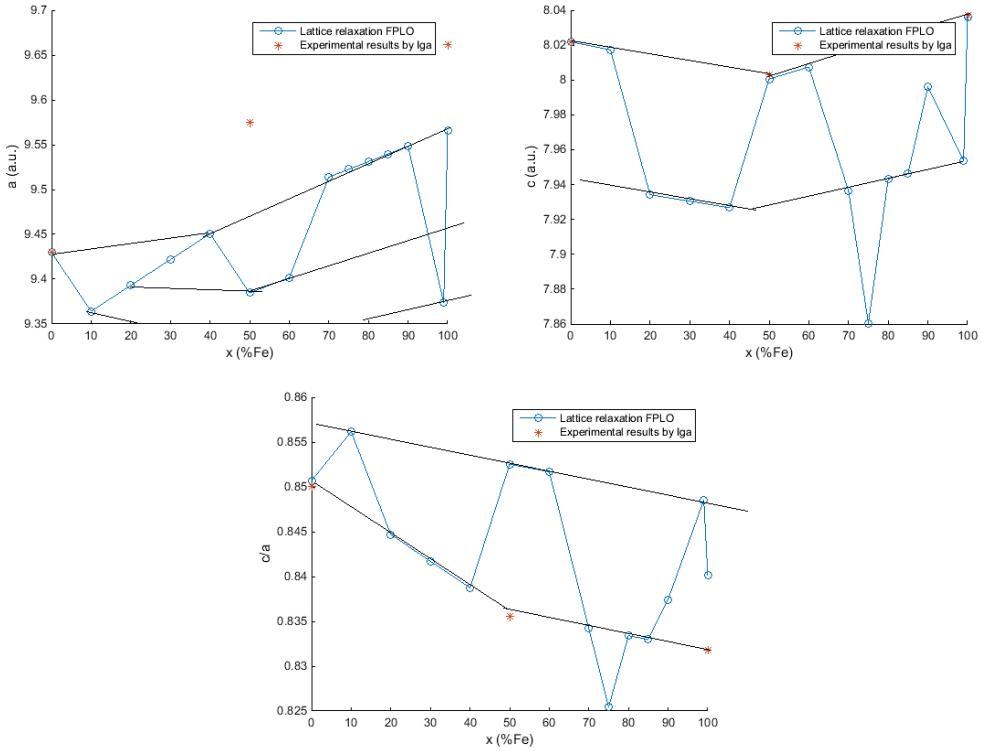

Figure 4.2. The lattice constants as a function of iron concentration and comparing with the experimental results by Iga with added black lines to illustrate the possible local minimum locations [5].

where a small change in the iron concentration corresponds to a similarly small change in lattice parameters. Looking at the difference between the points for 99% iron and 100% iron this is not the case. Instead the data points presented in figure 4.1 seem to form two or more bands so that the expected curves can be seen more or less parallel with each other as illustrated in figure 4.2. This suggests that the calculations have found local minima and that the results cannot be taken as is. Since the difference between the calculated results and the experimental results found by Iga [5] are small however these experimental results can be used instead with the remaining points being calculated by linear interpolation between these experimental results. The lattice constants being used for the purpose of this work will thus be the ones presented in figure 4.3.

4.2 Magnetic moment

It has already been shown that for high concentration of nickel $(Fe_xNi_{1-x})_2B$ has a very low saturation magnetization M [5] and any calculations done here should successfully reproduce that.

As can be seen in table 4.2 and figure 4.4 the magnetic moment does indeed go very low at high concentrations of nickel and becoming completely non-magnetic in the case Ni_2B. In the SPR-KKR calculation the magnetic

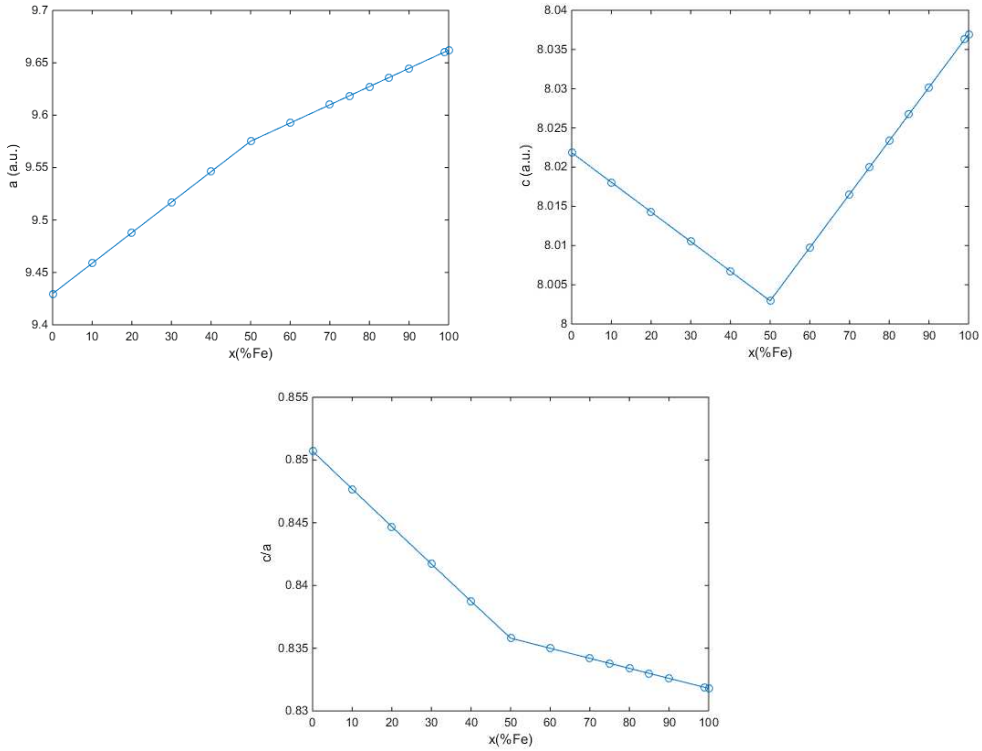

Figure 4.3. The lattice constants as a function of iron concentration and comparing with the experimental results by Iga with added black lines to illustrate the possible local minimum locations [5].

moment otherwise has a linear correlation with the iron concentration. By looking at the individual atom site magnetization it can be seen that the nickel is not magnetic or only slightly magnetic in any concentration and the only noteworthy magnetization comes from the addition of iron. This is in contrast to $(Fe_xCo_{1-x})_2B$ alloys, where both Fe and Co carry local magnetic moment across the whole range of concentrations.

4.3 MAE

In section 4.2 the magnetic moment for $(Fe_xNi_{1-x})_2B$ was shown. In order for a magnetic material with a uniaxial geometry to be useful however the magnetic moment needs to be along the uniaxial direction. Since the magnetization for high levels of nickel is very low it would be preferable if the uniaxial anisotropy would exist for higher concentrations of iron though it is known that the case Fe_2B does not have uniaxial anisotropy. In this work the MAE is defined so that a positive MAE corresponds to an easy axis magnetization. Figure 4.5 shows the MAE as a function of iron concentration.

In figure 4.5 it can be seen that $(Fe_xNi_{1-x})_2B$ indeed has uniaxial anisotropy for some values of x with the maximum MAE at $x = 0.8$. Table 4.3 and figures 4.6 and 4.5 shows that the value for the MAE reaches values around half that

Table 4.1. *The lattice constants of* $(Fe_xNi_{1-x})_2B$ *for some values of x.*

Composition	a(a.u.)	c (a.u.)	$\frac{c}{a}$
Ni_2B	9.43	8.02	0.85
$(Fe_{0.1}Ni_{0.9})_2B$	9.45	8.02	0.85
$(Fe_{0.3}Ni_{0.7})_2B$	9.52	8.01	0.84
$(Fe_{0.5}Ni_{0.5})_2B$	9.58	8.00	0.84
$(Fe_{0.7}Ni_{0.3})_2B$	9.61	8.02	0.83
$(Fe_{0.8}Ni_{0.2})_2B$	9.63	8.02	0.83
$(Fe_{0.9}Ni_{0.1})_2B$	9.64	8.03	0.83
Fe_2B	9.66	8.04	0.83

Table 4.2. *The magnetic moment of* $(Fe_xNi_{1-x})_2B$ *for some values of x.*

Composition	$\frac{c}{a}$	$M_{\text{SPR-KKR}}\left(\frac{\mu_B}{f.u}\right)$	$M_{\text{FPLO}}\left(\frac{\mu_B}{f.u}\right)$	$M_{\text{SPR-KKR}}\left(\frac{MA}{m}\right)$
Ni_2B	0.85	0.0000	0.0000	0.0000
$(Fe_{0.1}Ni_{0.9})_2B$	0.85	0.8611	0.0000	0.1533
$(Fe_{0.3}Ni_{0.7})_2B$	0.84	2.6192	1.8192	0.4657
$(Fe_{0.5}Ni_{0.5})_2B$	0.84	4.3486	4.0749	0.7726
$(Fe_{0.7}Ni_{0.3})_2B$	0.83	5.7702	6.1718	1.0056
$(Fe_{0.8}Ni_{0.2})_2B$	0.83	6.4445	6.6330	1.1181
$(Fe_{0.9}Ni_{0.1})_2B$	0.83	7.5217	7.0649	1.2917
Fe_2B	0.83	7.8858	7.4375	1.3426

of $(Fe_{0.7}Co_{0.3})_2B$ [6] and that it does so in the region of high iron concentration which can be seen in figure 4.4 and table 4.2 to be the region of higher saturation magnetization.

As can be seen by comparing figure 4.6 with figure 4.5 the SPR-KKR and FPLO calculations have rather poor agreement even at a qualitative level for high concentrations of nickel. The erratic nature around $x = 0.4$ in figure 4.6 implies that the VCA is a poor approximation for this material in part due to the fact that iron and nickel do not have adjacent atomic numbers.

4.4 DOS and bandstructure

In this section the density of states and band structure of $(Fe_xNi_{1-x})_2B$ for some specific values of x is presented. These values have been selected from figure 4.6 by looking at points of specific interest.

Two obvious points of interest are the end points Ni_2B and Fe_2B, being the ordered cases. In addition to that the cases $(Fe_{0.4}Ni_{0.6})_2B$ and $(Fe_{0.8}Ni_{0.2})_2B$ will be examined for being the minimum and the maximum points of the MAE curve in figure 4.5 respectively. And since the FPLO calculation showed no magnetic moment for the low iron concentration cases while the SPR-KKR showed a magnetic moment even at low non-zero concentrations of iron.

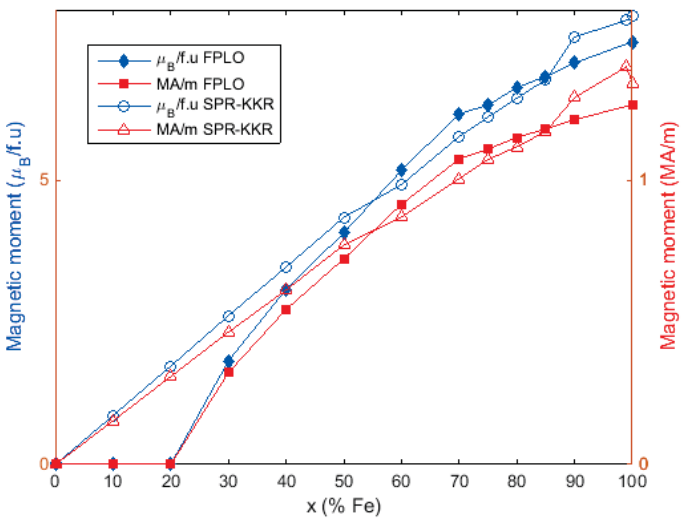

Figure 4.4. The saturation magnetization as a function of iron concentration calculated by the FPLO package and the SKPR-KKR package.

Table 4.3. *The MAE of* $(Fe_xNi_{1-x})_2B$ *for some values of x.*

Composition	$\frac{c}{a}$	$E_{MAE}^{SPR\text{-}KKR}\left(\frac{\mu eV}{f.u}\right)$	$E_{MAE}^{FPLO}\left(\frac{\mu eV}{f.u}\right)$	$E_{MAE}^{SPR\text{-}KKR}\left(\frac{MJ}{m^3}\right)$
Ni_2B	0.85	0.0	0.00	-0.00041
$(Fe_{0.1}Ni_{0.9})_2B$	0.85	-28.1	0.00	-0.11760
$(Fe_{0.3}Ni_{0.7})_2B$	0.84	-70.4	-251.5	-0.29421
$(Fe_{0.5}Ni_{0.5})_2B$	0.84	-56.9	-489.5	-0.23758
$(Fe_{0.7}Ni_{0.3})_2B$	0.83	4.1	10.2	0.01679
$(Fe_{0.8}Ni_{0.2})_2B$	0.83	74.4	219.2	0.30335
$(Fe_{0.9}Ni_{0.1})_2B$	0.83	-25.9	138.1	-0.10453
Fe_2B	0.83	-242.9	-148.6	-0.97188

Figure 4.7 show the DOS for these four cases. As for the band structure and Bloch spectral functions the dispersion relation of Ni_2B, Fe_2B, $(Fe_{0.4}Ni_{0.6})_2B$ and $(Fe_{0.8}Ni_{0.2})_2B$ is presented in figure 4.8.

As can be expected from the result that Ni_2B the result that the DOS is the same for spin up and spin down as can be seen from figure 4.7 is expected since this material is not spin polarized. For non-zero concentrations of iron exchange splitting occurs and the energy bands for the spin down electrons move up in energy.

Figure 4.8 show that the non-magnetic case has fewer bands around the Fermi energy than the ferromagnetic cases, which is to be expected. A more detailed study of the bandstructure in close neighborhood of the Fermi level would give some clues about the origins of the MAE. This is however beyond the scope of this thesis.

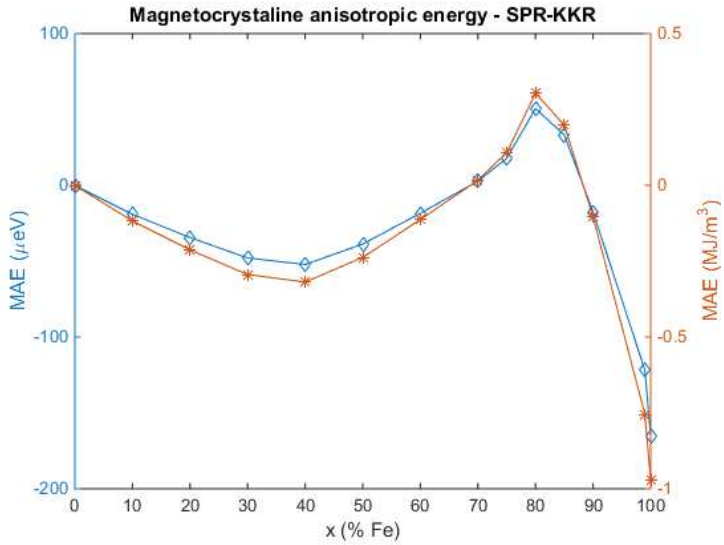

Figure 4.5. The MAE per formula unit as a function of iron concentration calculated by the SPR-KKR package. A positive MAE means a uniaxial anisotropy.

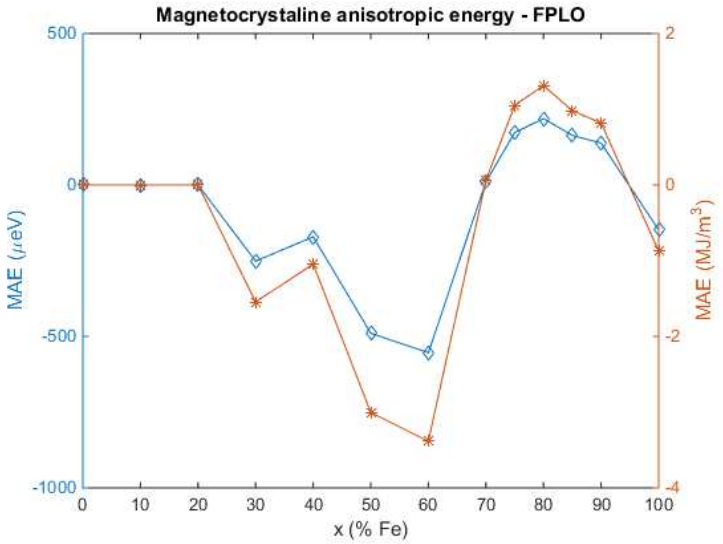

Figure 4.6. The MAE per formula unit as a function of iron concentration calculated by the FPLO package. A positive MAE means a uniaxial anisotropy.

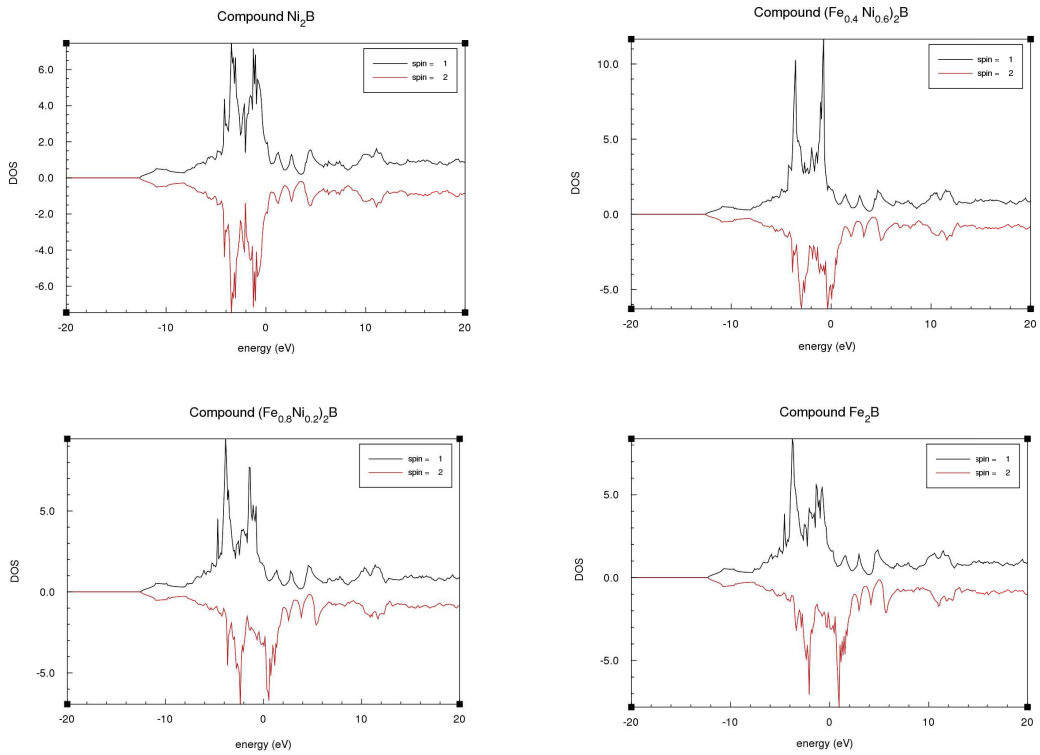

Figure 4.7. The DOS for Ni_2B (top left) , $(Fe_{0.4}Ni_{0.6})_2\,B$ (top right), $(Fe_{0.8}Ni_{0.2})_2\,B$ (bottom left) and Fe_2B (bottom right) calculated by the FPLO package.

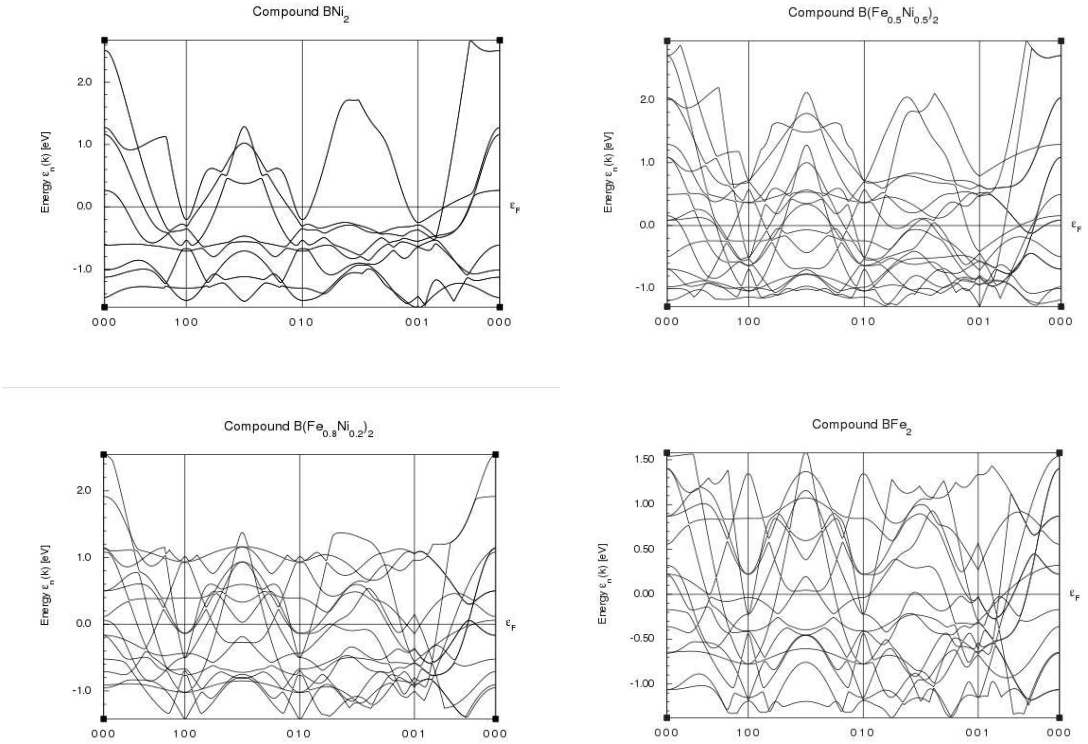

Figure 4.8. The dispersion relation for Ni_2B (top left) , $(Fe_{0.4}Ni_{0.6})_2\,B$ (top right), $(Fe_{0.8}Ni_{0.2})_2\,B$ (bottom left) and Fe_2B (bottom right) calculated by the FPLO package. Note that the cases $(Fe_{0.4}Ni_{0.6})_2\,B$ and $(Fe_{0.8}Ni_{0.2})_2\,B$ are to be seen as Bloch spectral functions where the bandwidth have been reduced to zero due to the VCA.

5. Conclusion

This work aims to give a theoretical background of permanent magnets and the computational methods used to study them. In addition to that theoretical calculation of the magnetization and MAE of $(Fe_xNi_{1-x})_2B$ has been presented. Apart from saturation magnetization and MAE the Curie temperature is an important property for a permanent magnet. Studying the Curie temperature is beyond the scope of this study however. A uniaxial anisotropy was found around $x = 0.8$ and though the MAE is lower than other $3d$-based magnetic materials it is comparatively cheap while still being higher than ferrite magnets and may still be worthy of further investigation since the magnetic moment was shown to be satisfactory at this concentration of iron and nickel.

Permanent magnets that are not made from rare-earth metals or other heavy elements is still an emerging field and the task is far from trivial. Trade-offs might need to be made concerning effectiveness or stability versus cost. Several candidates have been found however and many of them do seem like viable choices. Specifically it has been shown that a permanent magnet good enough for industrial application without containing materials heavier than the 3d transition metals is a viable pursuit.

References

[1] M. J. Kramer, R. W. McCallum, I. A. Anderson, and S. Constantinides. Prospects for non-rare earth magnets for traction motors and generators. *Journal of The Minerals, Metals & Materials Society*, 64(7):752–763, 2012.

[2] David Kramer. Concern grows over china's dominance of rare-earth metals. *Physics Today*, 63(5):22, 2010.

[3] J. M. D. Coey. Hard magnetic materials: A perspective. *Advances in Magnetics*, 47(12):4671–4681, 2011.

[4] P-K Tse. *China's rare-earth industry*. U.S. Geological Survey, 2011.

[5] Atushi Iga. Magnetocrystalline anisotropy in $(Fe_{1-x}Ni_x)_2B$ system. *Japanese Journal of applied physics*, 9:414–415, 1970.

[6] Alexander Edström. *Theoretical Magnet Design - From the electronic structure of solid matter to new permanent magnets*. Licentiate thesis, Uppsala Universitet, 2014.

[7] A. Edström, M. Werwiński, D. Iuşan, J. Rusz, O. Eriksson, K. P. Skokov, I. A. Radulov, S. Ener, M. D. Kuz'min, J. Hong, M. Fries, D. Yu. Karpenov, O. Gutfleisch, P. Toson, and J. Fidler. Magnetic properties of $(Fe_{1-x}Co_x)_2b$ alloys and the effect of doping by 5d elements. *Physical review B*, 92(17):174413, 2015.

[8] K. D. Belashchenko, L. Ke, M. Däne, L. X. Benedict, T. N. Lamichhane, V. Taufour, A. Jesche, S. L. Bud'ko, P. C. Canfield, and V. P. Antropov. Origin of the spin reorientation transitions in $(Fe_{1-x}Co_x)_2b$ alloys. *Applied Physics Letters*, 106(6):062408, 2015.

[9] W. Pauli. Zur Quantenmechanik des magnetischen Elektrons. *Zeitschrift für Physik*, 43(9-10):601–623, 1927.

[10] C. G. Darwin. Free motion in the wave mechanics. *Proceedings of the Royal Society A.*, 117(776):258–293, 1927.

[11] P. A. M. Dirac. The quantum theory of the electron. *Proceedings of the Royal Society A*, 117(778):610–624, 1928.

[12] P. A. M. Dirac. The quantum theory of the electron. part ii. *Proceedings of the Royal Society A.*, 118(779):351–361, 1928.

[13] R. Feder, F. Rosicky, and B. Ackermann. Relativistic multiple scattering theory of electrons by ferromagnets. *Zeitschrift für Physik B*, 52:31–36, 1983.

[14] P. Strange, J. Staunton, and B. L. Gyorffy. Relativistic spin-polarised scattering theory - solution of the single-site problem. *Journal of Physics C: Solid State Physics*, 17(19):3355–3371, 1984.

[15] G. Schadler, P. Weinberger, A. M. Boring, and R. C. Albers. Relativistic spin-polarized electronic structure of Ce and Pu. *Physical Review B*, 34(2):713–722, 1986.

[16] E. van Lenthe, J. G. Snijders, and E. J. Baerends. The zero-order regular approximation for relativistic effect: .The effect of spin-orbit coupling in closed shell molecules. *The Journal of Chemical Physics*, 105(15):6505–6516, 1996.

[17] R. L. Martin. All-electron relativistic calculations on AgH. an investigation of the Cowan-Griffin operator in a molecular species. *Journal of Physical Chemistry*, 87(5):750–754, 1982.
[18] H. Ebert, P Strange, and B. L. Gyorffy. The influence of relativistic effects on the magnetic moments and hyperfine fields of Fe, Co and Ni. *Journal of Physics F: Metal Physics*, 18(7):135–139, 1988.
[19] E. C. Stoner and E. P. Wohlfarth. A mechanism of magnetic hysteresis in heterogenous alloys. *Philosophcal transactions of the Royal Society of London A*, 240(826), 1948.
[20] S Chikazumi. *Physics of Ferromagnetism*. Oxford University Press, 1997.
[21] H. Ebert, D. Ködderitzsch, and J. Minár. Calculating condensed matter properties using the KKR-Green's function method - recent developments and applications. *Reports on Progress in Physics*, 74(9):095401, 2011.
[22] L. Szunyogh, B. Újfalussy, and P Weinberger. Magnetic anisotropy of iron multilayers on .Au(001): First-principles calculations in terms of the fully relativistic spin-polarized screened KKR method. *Physical Review B*, 51(15):9552–9559, 1995.
[23] W Koch and M. C. Holthausen. *A Chemist's Guide to Density Funcitonal Theory*. Wiley-VCH, 2001.
[24] J. C. Slater. A simplification of the hartree-fock method. *Physical Review*, 81(3):385–390, 1951.
[25] W. Kohn and L. J. Sham. Self-consistent equations including exchange and correlation effects. *Physical Review A*, 140(4):1133–1138, 1965.
[26] P. Hohenberg and W. Kohn. Inhomogeneous electron gas. *Physical Review B*, 136(3):864–871, 1964.
[27] T. L. Gilbert. Hohenberg-kohn theorem for nonlocal external potentials. *Physical Review B*, 12(6):2111–2120, 1975.
[28] J. Garza, R. Vargas, J. A. Nichols, and D. A. Dixon. Orbital energy analysis with respect to lda and self-interaction corrected exchange only potentials. *The Journal of Chemical Physics*, 114(2):639–651, 2001.
[29] P. M. Laufer and J. B. Krieger. Test of density-functional approximations in an exactly soluble model. *Phsyical Review A*, 33(3):1480–1491, 1986.
[30] J. P. Perdew and M. Levy. Physical content of the exact Kohn-Sham orbital energies: Band gaps and derivative discontinuities. *Physical Review Letters*, 51(20):1884–1887, 1983.
[31] A. I. Anisimov, F. Aryasetiawan, and A. I. Lichtenstein. First-principles calculations of the electronic structure and spectra of strongly correlated systems: the lda + u method. *Journal of Physics: Condensed Matter*, 9:767–808, 1997.
[32] A. Kabir, V. Turkowski, and T. S. Rahman. A DFT + nonhomogeneous DMFT approach for finite systems. *Journal of Physics: Condensed Matter*, 27(12):1–5, 2015.
[33] I. A. Nekrasov, V. S. Pavlov, and Sadovkii M. V. Consistent LDA' + DMFT - an unambiguous way to avoid double counting problem: NiO test. *JETP Letters*, 95(11):581–585, 2012.
[34] C. Stampfl, W. Mannstadt, R. Asahi, and A. J. Freeman. Electronic structure and physical properties of early transition metal mononitrides:

Density-functional theory lda, gga, and screened-exchange lda flapw calculations. *Physical Review B*, 63(15):1–11, 2001.
[35] Y. S. Mohammed, Y. Yan, H. Wang, K. Li, and X. Du. Stability of Ferromagnetism in Fe, Co, and Ni metals under high pressure with GGA and GGA+U. *Journal of Magnetism and Magnetic Materials*, 322(6):653–657, 2010.
[36] J. P. Perdew, K. Burke, and M. Ernzerhof. Generalized gradient approximation made simple. *Physical Review Letters*, 77(18):3865–3868, 1996.
[37] L. Bellache and D. Vanderbilt. Virtual crystal approximation revisited: Application to dielectric and piezoelectric properties of perovskites. *Physical Review B*, 61(12):7877–7882, 1999.
[38] P. Söderlind, O. Eriksson, and B. Johansson. Spin and orbital magnetism in Fe-Co and Co-Ni alloys. *Physical Review B*, 45(22):12911–12916, 1992.
[39] J. M. Schoen. Augmented-plane-wave virtual crystal approximation. *Physical Review*, 184(3):858–863, 1969.
[40] I. Turek, J. Kudrnovský, and K. Carva. Magnetic anisotropy energy of disordered tetragonal Fe-Co systems from ab initio alloy theory. *Physical Review B*, 86(17):174430, 2012.
[41] K. Koepernik and H. Eschrig. Full-potential nonorthogonal local-orbital minimum-basis band-structure scheme. *Physical Review B*, 59(3):1743–1757, 1999.
[42] P. Soven. Coherent-potential model of substitutional disordered alloys. *Physical Review*, 156(3):809–813, 1966.
[43] D. D. Johnson, D. M. Nicholson, F. J. Pinski, B. L. Györffy, and G. M. Stocks. Total-energy and pressure calculations for random substitutional alloys. *Physical Review B*, 41(14):9701–9716, 1990.
[44] J. L. Beeby. The density of electros in a perfect or imperfect lattice. *Proceedings of the Royal Society A*, 302:113–136, 1967.
[45] J. S. Faulkner and G. M. Stocks. Calculating properties with the coherent-potential approximation. *Physical Review B*, 21(8):3222–3244, 1980.
[46] A. M. Tsvelik. *Quantum Field Theory in Condensed Matter Physics*. Cambridge University Press, 2003.
[47] A. Ernst. *Multiple-scattering theory: new developments and applications*. Phd thesis, Martin-Luther-Universität Halle-Wittenberg, 2007.
[48] F. Yonezawa and K. Morigaki. Coherent potential approximation-basic concepts and applications. *Supplement of the Progress of Theoretical Physics*, 53, 1973.
[49] H Ebert. *A spin polarized relativistic Korringa-Kohn-Rostoker (SPR-KKR) code for Calculating Solid State Properties*. 2012.
[50] D. A. Biava, S. Ghosh, D. D. Johnson, W. A. Shelton, and A. V. Smirnov. Systematic, multisite short-range-order corrections to the electronic structure of disordered alloys from first principles: The KKR nonlocal CPA from the dynamical cluster approximation. *Physical Review B*, 72(11):113105, 2005.
[51] G. M. Stocks, W. M. Temmerman, and B. L. Gyorffy. Complete solution of the Korringa-Kohn-Rostoker Coherent-Potential-Aproximaiton equations: Cu-Ni alloys. *Physical Review Letters*, 41(5):339–343, 1978.
[52] J. Korringa. On the calculation of the energy of a Bloch wave in a metal. *Physica*, 13(6-7):392–400, 1947.

[53] W. Kohn and N. Rostoker. Solution of the Schrödinger equation in periodic lattices with an application to metallic lithium. *Physical Review*, 94(5):1111–1120, 1954.

[54] R. Zeller, P. H. Dederichs, B. Újfalussy, L. Szunyogh, and P. Weinberger. Theory and convergence properties of the screened .Korringa-Kohn-Rostoker method. *Physical Review B*, 52(12):8807–8812, 1995.

[55] I. Opahle, K. Koepernik, and H. Eschrig. Full-potential band-structure calculation of iron pyrite. *Physical Review B*, 60(20):14035–14041, 1999.

[56] N. W. Ashcroft and N. D. Mermin. *Solid State Physics*. Brooks/Cole, Belmont, USA, 1976.

[57] N. Papanikolaou, R. Zeller, and P. H. Dederichs. Conceptual improvements of the kkr method. *Journal of Physics: Condensed Matter*, 14(11):2799–2823, 2002.

[58] R. Zeller. An elementary derivation of Lloyd's formula valid for full-potential multiple-scattering theory. *Journal of Physics: Condensed Matter*, 16(36):6453–6468, 2004.

[59] B. Drittler, M. Weinert, R. Zeller, and P. H. Dederichs. First-principles calculation of impurity-solutions energies in Cu and Ni. *Physical Review B*, 39(2):930–939, 1989.